Diagnosing ozone-NOx-VOC sensitivity and revealing causes of ozone increases in China based on 2013-2021 satellite retrievals

Jie Ren[1], Shaodong Xie[1]

[1]State Key Joint Laboratory of Environmental Simulation and Pollution Control, College of Environmental Sciences and Engineering, Peking University, Beijing, 100871, China

Correspondence to: Shaodong Xie (sdxie@pku.edu.cn)

Abstract. Particulate matter ($PM_{2.5}$) concentrations in China have decreased significantly in recent years, but surface ozone (O_3) concentrations showed upward trends at more than 71% of air quality monitoring stations from 2015 to 2021. To reveal causes of O_3 increases, O_3 production sensitivity is accurately diagnosed by deriving regional threshold values of satellite tropospheric formaldehyde-to-NO_2 ratio ($HCHO/NO_2$), and O_3 responses to precursors changes are evaluated by tracking volatile organic compounds (VOCs) and NOx with satellite HCHO and NO_2. Results showed that the $HCHO/NO_2$ ranges of transition from VOC-limited to NOx-limited regimes vary apparently among Chinese regions. VOC-limited regimes are widespread found over megacity clusters (North China Plain, Yangtze River Delta, and Pearl River Delta) and concentrated in developed cities (such as Chengdu, Chongqing, Xi'an, and Wuhan). NOx-limited regimes dominate most of the remaining areas. From 2013 to 2021, satellite NO_2 and HCHO columns showed an annual decrease of 3.7% and an increase of 0.1%, respectively, indicating an effective reduction in NOx emissions but a failure reduction of VOC emissions. This finding further shows that O_3 increases in major cities occur because the Clean Air Action Plan only reduces NOx emissions without effective VOC control. Two cases in Beijing and Chengdu also verified that NOx reduction alone or VOC increase leads to O_3 increases. Based on the O_3–NOx–VOC relationship by satellite NO_2 and HCHO in Beijing, Chengdu, and Guangzhou, the ozone concentration can be substantially reduced if the reduction ratio of VOCs/NOx is between 2:1 and 4:1.

Atmospheric
Chemistry
and Physics
Discussions

1 Introduction

China has been dedicating to fighting against air pollution in the past years. Since the Chinese government implemented the Air Pollution Prevention and Control Action Plan in 2013, the ambient concentration of particulate matter with aerodynamic diameter of <2.5 μm ($PM_{2.5}$) has decreased significantly (Jiang et al., 2020; Xiao et al., 2021); however, ozone (O_3) pollution remains severe or even continues to worsen at least until 2019 (Lu et al., 2020; Zhao et al., 2020). Ozone pollution has restricted the continuous improvement of China's air quality. Thus, it has attracted widespread attention from the government, scientists, and the public.

Tropospheric ozone is produced by photochemical oxidation of volatile organic compounds (VOCs) in the presence of nitrogen oxides (NOx: NO + NO_2) (Atkinson, 2000). However, the O_3 responses to NOx and VOC reduction are not linear. The O_3 formation throughout much of the troposphere is largely controlled by the availability of NOx (NOx-limited), but in regions with high NOx emissions, such as metropolitan areas, O_3 formation can be VOC-limited or transform between regimes (Sillman and He, 2002; KLEINMAN, 1994). A VOC-limited regime means that reducing VOC emissions can result in low O_3 production; in the presence of high NOx, reduction of NOx emissions alleviates ozone titration and even leads to ozone increases (Sillman, 1999). Local O_3 formation chemistry determines the effect of changes in VOC and NOx emissions on ozone concentrations.

Various ground-based observation (Nelson et al., 2021; Tan et al., 2018) and model-based methods (Shen et al., 2021; Wang et al., 2019; Wang et al., 2021) have been applied to study O_3-NOx-VOC sensitivity. The field observation methods can provide accurate in-situ diagnoses of O_3 sensitivity but are limited in temporal and spatial extent (Wang et al., 2017). Air quality model-based methods provide descriptions across time and space. However, uncertainties mainly from emission inventories, as well as meteorological factors and photochemical reactions reduce the accuracy of simulation results (Liu and Shi, 2021). Based on the continuous global observations of formaldehyde (HCHO) and nitrogen dioxide (NO_2) by satellite spectrometers, the space-based HCHO-to-NO_2 ratio can be used as an indicator of O_3 sensitivity because HCHO/NO_2 theoretically reflects the relative availability of NOx and total organic reactivity to hydroxyl radicals (SILLMAN, 1995). This satellite-based method can provide global-scale photochemical information with good time continuity and little human disturbance, which governments and policymakers are keen to know.

In China, there have been many studies exploring O_3-NOx-VOCs sensitivity based on satellite-retrieved HCHO/NO_2 (Jin and Holloway, 2015; Li et al., 2021). They are based on thresholds derived from earlier work that used air quality models to link HCHO/NO_2 with surface O_3 sensitivity over the United States (Martin et al., 2004; Duncan et al., 2010; Choi et al., 2012). However, the model approach can be biased because modelled and observed HCHO columns, NO_2 columns, and surface O_3 often disagree. Jin et al. (2020) derived the threshold values from observations and found the transition in O_3 formation regimes occurs at higher HCHO/NO_2 value than previously determined from models. In addition, the range of HCHO/NO_2 marking transitional regimes varies regionally because of the differences in meteorological conditions, ozone levels, and precursor composition (Schroeder et al., 2017). The threshold extracted in the United States may not be suitable

55 for China and a uniform value may not be applicable to all Chinese cities. Consequently, the transitional regime range of HCHO/NO_2 across China requires further in-depth analysis to diagnose ozone–precursor sensitivity.

O_3–NOx–VOC sensitivity and changes in VOC and NOx emissions directly affect ozone concentrations. Nationwide annual estimates of anthropogenic VOC and NOx emissions in China show different trends from 2013 to 2019, with successive large decreases in NOx but only slight changes in VOC (Zheng et al., 2018a; Simayi et al., 2022). Previous

60 studies showed that the rapid reduction of NOx emission increases the surface ozone levels in urban regions (Ren et al., 2021; Yang et al., 2019). In addition, some model simulations suggested that the notable drop of $PM_{2.5}$ is the most crucial factor leading to the O_3 increment in China because of the release of HO_2 from its uptake on $PM_{2.5}$ (Li et al., 2019). However, this idea is highly controversial (Tan et al., 2020). In order to reveal the relationship between ozone increases and changes in its precursors' emissions, satellite-based NO_2 and HCHO can be used as visual, timely, and high-resolution trackers of NOx and

65 VOCs emissions, respectively (Duncan et al., 2010).

In this study, we first take advantage of the Chinese extensive air quality monitoring network to assess the latest trends in ozone concentrations comprehensively. The threshold values that mark the O_3 formation transition are derived and used to identify the O_3–NOx–VOC sensitivity by matching satellite-based HCHO/NO_2 with ground-based O_3 measurements across China and in different regions. The effects of precursors on ozone and the causes of ozone increase are explored by

70 combining ozone production regimes with interannual variations in NOx and VOC emissions inferred from tropospheric NO_2 and HCHO vertical columns. Special measures for plague prevention and work resumption during the COVID-19 pandemic also provide an opportunity to assess O_3 response to changes in VOC and NOx emissions. Furthermore, the optimal VOCs/NOx reduction ratio is probed in three typical cities, Beijing, Chengdu, and Guangzhou, based on the relationships between O_3 and HCHO/NO_2, to provide scientific support for future O_3 pollution control.

75 **2 Data and Methodology**

2.1 Ground-Based Observation of O_3 and NO_2

The Chinese nationwide air quality monitoring network provides surface O_3 and NO_2 data. Since 2015, more than 1400 sites have covered more than 330 cities across the country. The nationwide hourly O_3 and NO_2 concentration data in Chinese cities in 2014–2021 were obtained from the National Urban Air Quality Real-Time Publishing Platform

80 (http://106.37.208.233:20035/).

O_3 and NO_2 mass concentrations were reported in $\mu g\ m^{-3}$ and unified to the reference state (298.15 K, 1013.25 hPa). Extensive data quality controls were applied to eliminate unreliable observed outliers following the method of previous studies (Lu et al., 2018). The average concentration of all national-controlled sites in a city was regarded as the city's O_3 and NO_2 level.

2.2 Satellite Observations of O_3 Precursors

Given the short lifetime of NOx, the high NO_2/NOx ratio in the boundary layer, and the fact that HCHO is an intermediate in the oxidation reactions of various VOCs and is approximately proportional to the total rate of VOC reactions with OH radicals (Duncan et al., 2010), current satellite-based spectrometers have provided continuous global observations for two species indicative of O_3 precursors, namely, NO_2 for NO_X (Lamsal et al., 2014; Martin, 2003) and HCHO for VOCs (Shen et al., 2019; Zhu et al., 2014).

Satellite products of tropospheric NO_2 and HCHO vertical columns are retrieved from two satellite instruments: Ozone Monitoring Instrument (OMI) and Tropospheric Monitoring Instrument (TROPOMI). The high spatial resolution (24×13 km^2 for OMI and 5×3.5 km^2 for TROPOMI) allows for the observation of fine details of atmospheric parameters. The overpass time (13:40–13:50 and 13:30 local time) is well suited to detect the O_3 formation sensitivity when O_3 photochemical production peaks, the boundary layer is high, and the solar zenith angle is small, thereby maximizing instrument sensitivity to HCHO and NO_2 in the lower troposphere (Jin et al., 2017).

The OMI data are developed under the Quality Assurance for Essential Climate Variables (QA4ECV) project. The vertical profiles used for QA4ECV products are obtained from the TM5-MP chemical transmission mode (Williams et al., 2017). The spatial resolutions of OMI NO_2 and OMI HCHO are 0.125° and 0.05°, respectively. The TROPOMI data from the Earth Engine Data Catalog are based on the algorithm developments for the QA4ECV reprocessed dataset for OMI, and have been further optimized. The TROPOMI data are processed with a spatial resolution of 0.01°. The same chemistry transport model for HCHO and NO_2 is better suited for analysing their ratio than products developed with different prior profiles.

To study the interannual variations in HCHO, NO_2, and $HCHO/NO_2$, the satellite records are based on TROPOMI observations for the years after 2019 and harmonized OMI observations for 2013–2018. Satellite retrievals must be harmonized to account for differences in any instrumental offset. OMI HCHO and NO_2 data are adjusted with reference to TROPOMI because the latter has a finer spatial resolution and attains a smaller deviation than the former. The instrumental difference between OMI and TROPOMI is estimated as the difference between the two at OMI coarse resolution for the overlapping months. The difference is considered independent of the instrumental resolution. TROPOMI data consistent with the coarse resolution of OMI data are obtained. The difference between them at month m and grid cell x is $\Delta D\_(x,m)$. The adjusted OMI data at year yr month m and grid cell x ($D\_{OMIadj}(x,yr,m)$) are estimated as the sum of the original OMI data ($D\_{OMI}(x,yr,m)$) and $\Delta D\_(x,m)$.

2.3 Connecting Satellite $HCHO/NO_2$ with Ground-Based O_3 Observations

TROPOMI data are aggregated by sampling gridded NO_2 and HCHO columns consistent with the ground-based observations of O_3. O_3 concentrations are averaged at all available sites every half month for the warm season (April to September) from 2019 to 2021. O_3 measurements at 13:00 to 14:00 local time are selected to match the TROPOMI overpass

time. TROPOMI-retrieved NO_2 and HCHO columns are sampled every half month over O_3 sites for the same period, yielding nearly 100 000 paired observations. In addition, China is divided into nine regions to evaluate the satellite-based HCHO/NO_2 and study the O_3 production regimes from 2013 to 2021. Based on satellite and surface observations, the response of O_3 concentrations and changes in O_3 precursors are compared in two typical cities, Beijing and Chengdu, during the COVID-19 pandemic in spring 2020 to assess the effectiveness of the O_3 production regimes for satellite HCHO/NO_2 capture.

3 Results and Discussion

3.1 Surface Ozone Trends

The ozone concentrations averaged from 367 cities with monitoring sites in China from 2015 to 2021 are shown in Fig. 1a. The three metrics include the maximum 6-month MDA8 ozone running average (MMA6-MDA8) and the 90th and 99th percentiles of the annual distribution of MDA8-O_3 (MDA8-90th, MDA8-99th), following the definition in World Health Organization global air quality guidelines (World Health Organization, 2021) and Chinese ambient air quality standards (GB 3095-2012). The three metrics increased at 2.3 (2%), 2.5 (2%), and 2.3 (1%) $\mu g\ m^{-3}\ year^{-1}$ in 2015-2021. Moreover, they significantly increased at 4.6 (5%), 5.6 (4%), and 5.4 (3%) $\mu g\ m^{-3}\ year^{-1}$ (all with $p < 0.05$) in 2015-2019, based on the linear trend estimate.
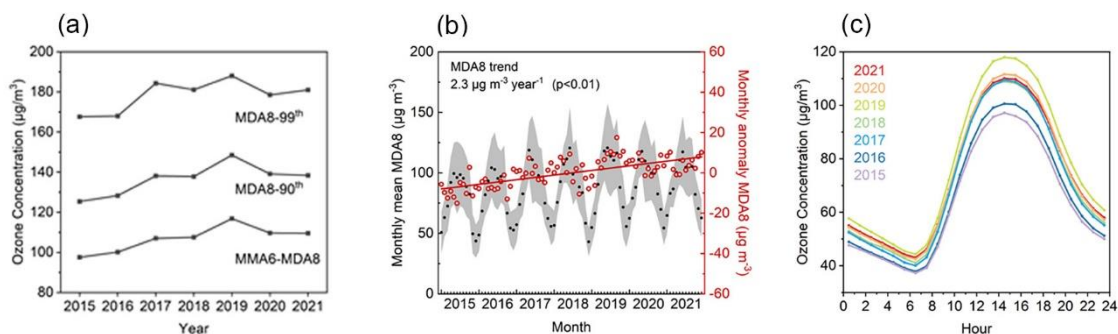

Figure 1: Surface ozone concentrations in China. (a) MDA8-99th, MDA8-90th, MMA6-MDA8, and (b) monthly average (black dots, left axis) and anomaly (circle, right axis) of MDA8 ozone concentrations averaged from all 367 cities with monitoring sites in 2015–2021. Gray shading: mean value ± standard deviation across all cities for each month. Solid line: linear fitted curve. (c) Ozone diurnal cycles from April to September.

The time series of the monthly mean MDA8 ozone in 2015–2021 is shown in Fig. 1b. Based on the monthly anomalies (the difference between the observed monthly mean and the 7-year monthly mean for the same month), MDA8 ozone levels increased by 2.3 $\mu g\ m^{-3}\ year^{-1}$ (3.0% $year^{-1}$, $p < 0.01$) averaged from all cities. The increases are also exhibited rapidly before 2019, with 3.5 $\mu g\ m^{-3}\ year^{-1}$ (4.5% $year^{-1}$, $p < 0.01$). The daytime and nighttime mean ozone levels show similar trends. In 2015–2019, the maximum and minimum hourly average concentration increased from 97.1 to 117.9 $\mu g\ m^{-3}$ and

5

from 37.3 to 44.3 µg m^{-3}, respectively, based on the mean April to September ozone diurnal variation, as shown in Fig. 1c. Overall, the average ozone concentration shows an increasing trend from 2015 to 2021, although it has decreased in the last two years compared to the peak in 2019.

(a) MDA8-90 (µg m^{-3})

(b) MDA8-90 trend (µg m^{-3} yr^{-1})
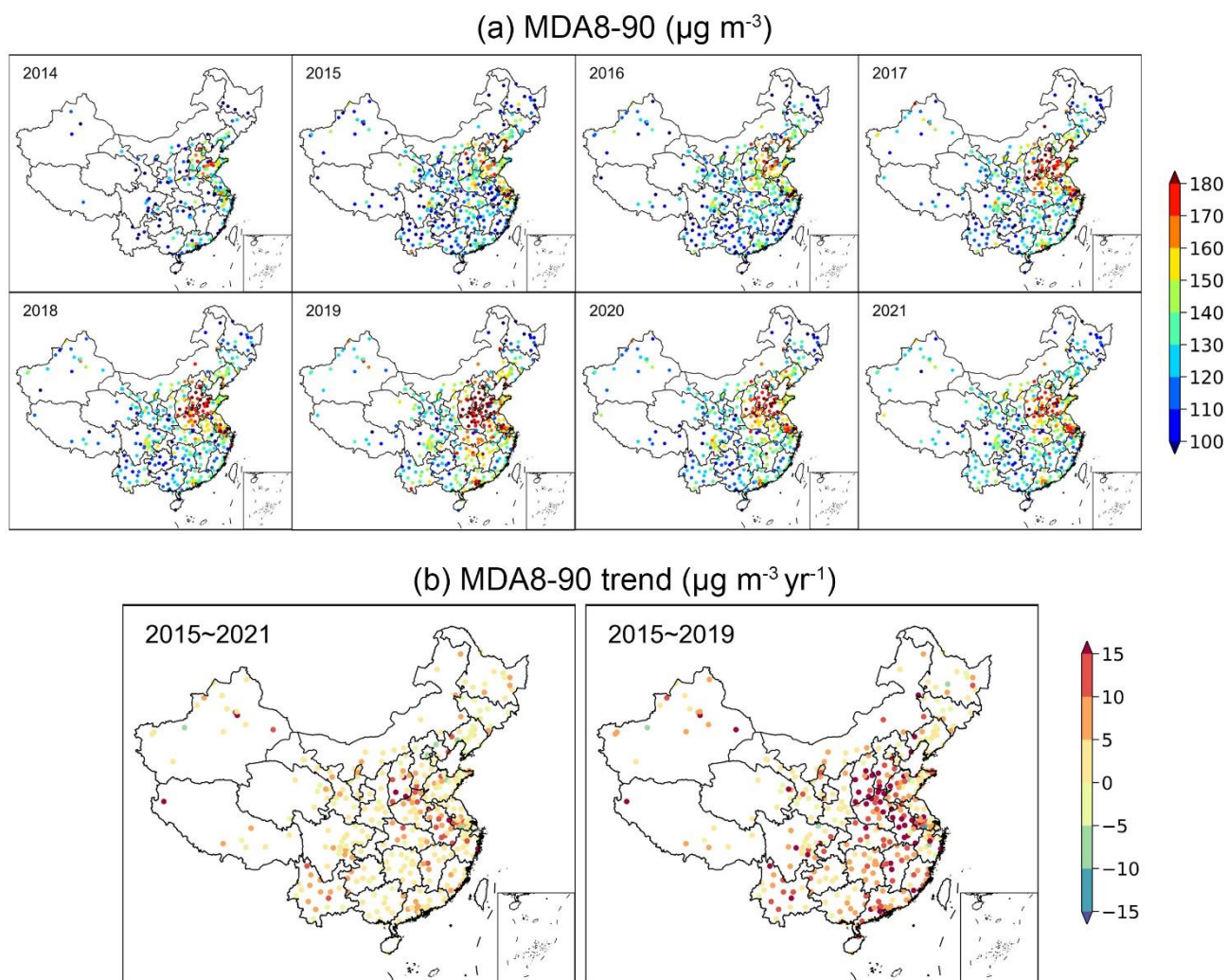
145

Figure 2: Spatiotemporal distributions of MDA8-90th ozone in China from 2014 to 2021, and trends for 2015–2019 and 2015–2021.

The spatial patterns of MDA8-90th and their trends for approximately 367 cities in 2014–2021 are shown in Fig. 2. The cities with high ozone levels are widely distributed in eastern and central China, where intensive anthropogenic emissions are located. Distinct exacerbation of ozone pollution can be observed from 2014 to 2019. The locations and definitions of the key regions are shown in Fig. S1. In 2014–2015, sites with MDA8-90th greater than 160 µg m^{-3} were concentrated near the Beijing-Tianjin-Hebei and the Yangtze River Delta (YRD) megacity clusters. By 2019, ozone hot spots extended westward

to the Fenwei Plain and southward to the central Yangtze River Plain. During the 6 years, the ozone concentration has increased almost everywhere in China, particularly in the North China Plain (NCP) and the central Yangtze River Plain. In 2020 and 2021, ozone pollution was alleviated; the level of which is equivalent to the level of ozone pollution in 2017–2018.

155 O_3 concentration decreases in major key regions, including the North China Plain, Pearl River Delta (PRD), and Sichuan Basin (SCB).

The percentage of sites with MDA8-90th ozone higher than 160 μg m^{-3}, the Chinese grade II national air quality standard, increased from 15.0% in 2015 to 39.3% in 2019 and then decreased to 23.0% in 2021. The percentage of sites with increasing ozone trends was 83.1% in 2015–2019 and 71.8% in 2015–2021. From a national perspective, widespread surface

160 ozone increases occurred in Chinese cities during 2015–2019. Moreover, decreases have been observed in the last 2 years.

3.2. Ozone–NOx–VOC sensitivity over China

3.2.1 Ozone–NOx–VOC Chemistry Captured by Satellite-Based HCHO/NO₂

Ozone formation can be limited by NOx, VOCs, or both. Satellite-based HCHO and NO_2 columns are evaluated whether they can capture the nonlinearities in O_3–VOCs–NOx chemistry. Figure 3a, similar to classic ozone isopleths

165 typically generated with models (Sillman et al., 1990; Pusede et al., 2015), shows the in situ O_3 concentration as a function of TROPOMI NO_2 and HCHO derived solely from observations.
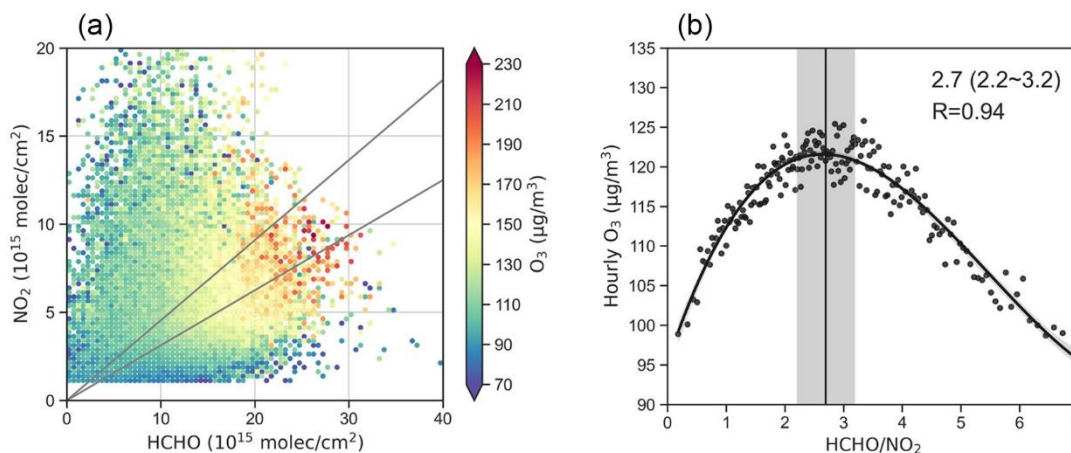
Figure 3: (a) O₃ concentration as a function of TROPOMI HCHO and NO₂. All surface hourly O₃ observations (13:00 to 14:00 local time) averaged over each half month from April to September 2019–2021 are aggregated based on the corresponding TROPOMI HCHO and NO₂ (interval: 0.5 unit × 0.25 unit). The black lines delineate the TROPOMI HCHO/NO₂ values of 2.2 and 3.2. (b) O₃ concentration as a function of TROPOMI HCHO/NO₂. O₃ average concentration is calculated by first matching hourly O₃ observations with TROPOMI HCHO/NO₂ for each half of the month, dividing these paired observations into 200 bins based on HCHO/NO₂, and then calculating the O₃ average concentration (y axis) for each TROPOMI HCHO/NO₂ bin (x axis). The solid line is fitted with third-order polynomial curves, and the shading indicates 95% confidence intervals. The vertical lines indicate the maximum of the fitted curve, and the vertical shading represents the range with the curve slope from −3 to +3 (regime transition).

Consistent with O_3 isopleths, O_3 concentration is a non-linear process in relation to NO_2 and HCHO, as shown in Fig. 3a. Three regimes can be roughly identified. When HCHO is low and NO_2 is relatively high, the O_3 concentration is high at

lower NO_2 or higher HCHO, indicating VOC-limited (or NOx-saturated) chemistry. When NO_2 is low and HCHO is relatively high, the O_3 concentration increases with increasing NO_2, indicating NOx-limited chemistry. When both NO_2 and HCHO are high, O_3 concentration peaks and increases with both increasing NO_2 and HCHO. However, the division between the three regimes is uncertain and ambiguous, which may be influenced by other factors such as different meteorology, noisy satellite retrievals, the spatial mismatch between gridded satellite observations and point measurements on the ground, and lack of statistical power to calculate average concentrations in some intervals due to small sample sizes. Despite these uncertainties, Figure 3a qualitatively illustrates the nonlinear relationship between O_3 and satellite NO_2 and HCHO, similar to the overall O_3-NOx-VOC chemistry.

After the qualitative approach is established, the HCHO/NO_2 thresholds that mark the O_3 transitional regime are then derived by calculating the average ozone concentration for a given TROPOMI HCHO/NO_2 and examining their statistical relationships in China and the different regions within it. Empirical relationships are investigated by applying second-order and third-order polynomial models (Jin et al., 2020) to the observations over all cities in China. The third-order polynomial model is used to derive the maximum mean O_3 concentration (the peak of the curve in Fig. 3b) because it fits the data with the high correlation coefficient better than the second-order model does. Assuming that the peak of the curve (with a slope of 0) marks the transition from VOC-limited to NOx-limited regimes (Pusede and Cohen, 2012), the transitional regime (mixed sensitive regime) is defined as the range with a slope between −3 and +3.

The aggregation of the overall available observations used in Fig. 3a shows that the O_3 concentration peaks at HCHO/NO_2 are equal to 2.7, with the transitional regime between 2.2 and 3.2. A separate evaluation for nine regions also reveals the strong nonlinear relationships between the O_3 concentration and TROPOMI HCHO/NO_2, despite differences in the overall O_3 concentrations. The Pearson correlation coefficient between the fitted third-order polynomial curve and the data is generally more than 0.73, except for Inner Mongolia (0.59). The HCHO/NO_2 marking the regime transition varies among these regions (Table 1 and Fig. S2), with the highest in Shanxi-Shaanxi-Henan [3.7 (3.2–1.3)] and the lowest in Heilongjiang-Jilin-Liaoning [2.0 (1.2–3.2)]. Different cities respond differently to changes in NOx and VOC emissions. This varied response is also reflected in different thresholds for other photochemical indicators (Liu and Shi, 2021; Wang et al., 2017) or patterns of O_3 isopleths (Shen et al., 2021). This difference among regions may reflect environmental conditions (Liu and Shi, 2021), such as radiation intensity and surface temperature.

Atmospheric
Chemistry
and Physics
Discussions

Table 1. HCHO/NO₂ threshold values between O₃ production regimes in nine Chinese regions

| Region	Correlation coefficient [a]	HCHO/NO$_2$ [b]	Transitional regime
Beijing-Tianjin-Hebei-Shandong	0.93	3.4	3.0–3.8
Shanxi-Shaanxi-Henan	0.93	3.7	3.2–4.3
Shanghai- Jiangsu-Zhejiang-Anhui	0.85	2.7	2.2–3.3
Jiangxi-Hubei-Hunan-Fujian	0.76	3.2	2.2–4.7
Guangdong-Hong Kong-Macao- Guangxi-Hainan	0.82	3.2	2.7–3.8
Sichuan-Chongqing- Guizhou-Yunnan	0.73	3.2	2.5–4.3
Gansu-Ningxia-Qinghai-Tibet-Xinjiang	0.74	3.0	2.2–4.5
Inner Mongolia	0.59	2.5	1.9–3.4
Heilongjiang-Jilin-Liaoning	0.82	2.0	1.2–3.2

205   [a] The Pearson correlation coefficient between the fitted third-order polynomial curve and the data.

[b] HCHO/NO$_2$ value at the maximum of the fitted curve (peak O$_3$ concentration).

The HCHO/NO$_2$ thresholds in the present study are higher than the previously reported model-based values (Jin et al., 2017; Martin et al., 2004; Duncan et al., 2010). Thus, this observation-based method indicates that O$_3$ production tends to be VOC limited at the same HCHO/NO$_2$. This discrepancy stems from the different approaches linking HCHO/NO$_2$ to O$_3$

210   production regimes. Previous modelling studies derived thresholds by simulating the response of surface O$_3$ to the overall reductions in NOx or VOC emissions. Moreover, these thresholds were derived from the study area in the United States, which best represents regional rather than local O$_3$-NOx-VOC sensitivities (Martin et al., 2004; Jin et al., 2017). Thresholds derived with in situ observations in China take full account of the local O$_3$ chemistry.

3.2.2 Spatial Distribution of O₃ Production Regimes

215   The derived HCHO/NO$_2$ thresholds were used to identify the O$_3$ production regimes over China from April to September 2013–2021. Based on the same HCHO/NO$_2$ threshold across China (2.2–3.2, Fig. S3) and different thresholds for different regions (Fig. 4 and S4), two methods yield similar spatial distributions of O$_3$ sensitivity. However, the regional approach suggests that O$_3$ production tends to be VOC limited because the HCHO/NO$_2$ thresholds derived in many key regions individually are higher than the national overall threshold.
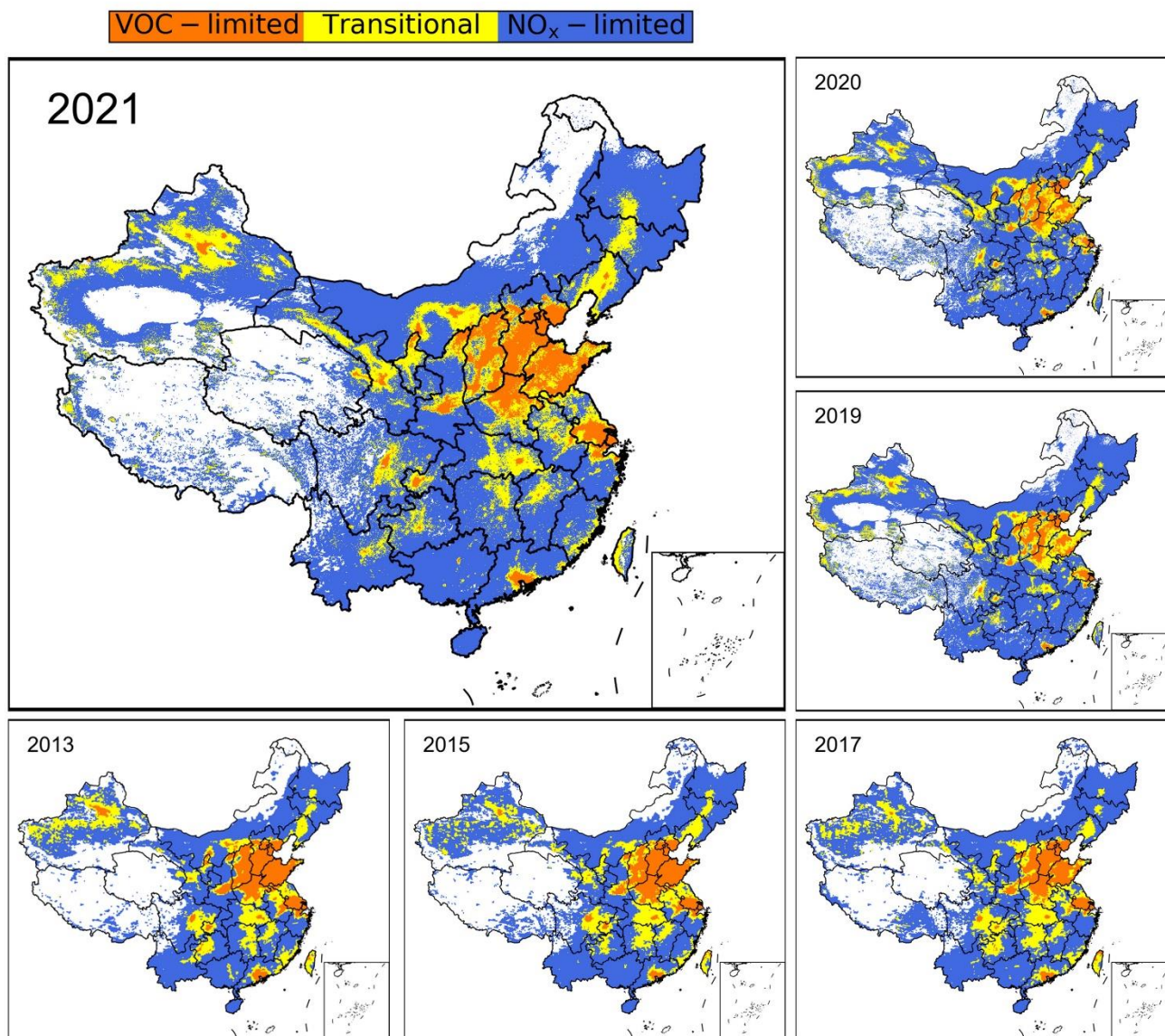
Figure 4: Ozone sensitivity classification over China from April to September 2013, 2015, 2017 and 2019–2021 using different HCHO/NO₂ thresholds in different regions. Only polluted regions are displayed (defined as average TROPOMI NO₂ columns higher than 1.0×10^{15} molecules/cm².

As shown in Fig. 4, the NOx-limited regime dominates in most regions from April to September. VOC-limited chemistry exists in urban areas of almost every province, with transitional regimes occurring around the VOC-limited regimes in wide urban and suburban areas. Widespread VOC-limited and transitional regimes are observed over major megacity clusters. In the North China Plain, the VOC-limited regimes are distributed in Beijing and most regions in the provinces of Hebei, Shanxi, Henan, and Shandong. Transitional regimes control almost all the remaining regions, except for

Atmospheric
Chemistry
and Physics
Discussions

individual cities in northern Hebei and southwestern Henan. The percentages of VOC sensitive regime and the transitional
230 regime are 59.2% and 26.7% in 2021 (Table S1). In the Yangtze River Delta, the VOC-limited regimes are found in some
developed urban cities including Shanghai, some cities in southern Jiangsu Province (such as Suzhou, Wuxi, and most of
Nanjing and Nantong) and Zhejiang Province (Jiaxing, urban of Hangzhou and Ningbo). VOC-limited and transitional or
mixed regimes occupy 23.5% and 31.4% of the total grid cells (Table S1). In the Pearl River Delta and surrounding areas
(Guangdong Province), VOC-limited regimes (8.0%) and transitional regimes (11.0%) control Shenzhen, Dongguan, Foshan,
235 Zhongshan, Zhuhai, most of Guangzhou, and some other urban areas, whereas NOx-sensitive regimes dominate most of the
remaining cities. In addition, extensive VOC-limited and transitional regimes occur in developed cities of Sichuan Basin
(urban centres of Chongqing and Chengdu), Shaanxi Province (Xi'an), Hubei Province (Wuhan), and other regions.
Compared with previous studies (Jin and Holloway, 2015; Wang et al., 2019), the results of this study are slightly different.
The areas dominated by VOC-limited and transitional regimes in China are expanded, especially in NCP; while in the
240 southern region (e.g., Guangdong Province), VOC-sensitive regimes are only concentrated in major cities.

Air quality monitoring sites are generally located in built-up areas of cities, representing the environment in which
people live. The ozone sensitivity regime of all monitoring sites' locations based on $HCHO/NO_2$ and the O_3 MDA8-90th in
2021 are shown in Fig. S5. VOC-limited and transitional regimes dominate O_3 formation at 86.2% of the sites, with VOC-
limited chemistry accounting for 52.5%.

245 The comparison of O_3 sensitivities from 2013 to 2021 (Fig. 4 and S4) shows a slight change in the trends of individual
regions from VOC-limited regimes to transitional regimes or from transitional regimes to NOx-limited regimes as a result of
NOx reduction. However, there has been no remarkable change in China as a whole. The changes in VOC and NOx
emissions in recent years have not led to the transition in the spatial distribution of the O_3 production regime defined by our
$HCHO/NO_2$ thresholds.

250 **3.3 Effects of Interannual Variations in Ozone Precursors**

Based on the non-linear relationship of O_3–NOx–VOC, the changes in ozone precursors is the direct factor affecting
ozone level. Ground-based measurements of NO_2 and satellite-based NO_2 columns are used to indicate the changes in NOx
emissions. As shown in Fig. 5a and S6, NO_2 is concentrated over urban areas and industrial cities, particularly in megacity
clusters, such as the NCP, YRD, and PRD, and large cities, such as Wuhan (in Hubei) and Xi'an (in Shaanxi). Satellite
255 observations show large NO_2 decreases from 2013. This finding is consistent with previous studies (Wang et al., 2019; Lin et
al., 2019). Moreover, the decrease is more than 2.8% per year in half of the grids. Figure 5b shows that the average annual
reduction in satellite NO_2 in eastern China is 3.7% (0.18×10^{15} molecules cm^{-2}, $p < 0.01$). A reverse increase has occurred in
the last 2 years, mainly in winter. Figure S7 shows similar trends in surface NO_2 concentrations and satellite-based NO_2
columns averaged in April–September from 2015 to 2021. More than 75% of the cities show negative trends in surface NO_2
260 levels (and 22% with $p < 0.05$), and nearly 73% of the grids show decreases in satellite NO_2 columns. Strong and consistent

decreases in high-value areas, particularly the NCP, as well as YRD, PRD, and SCB, have been observed in the last 9 years. The mean NO_2 in NCP has decreased by 0.59×10^{15} molecules cm^{-2} $year^{-1}$ (5.0%, $p < 0.01$) from 2013 to 2021.

The variations in anthropogenic VOCs primarily drive the temporal patterns of satellite HCHO columns over China

265 (Shen et al., 2019). Figures 6a and S6 compare the HCHO columns from April to September 2013–2021. As expected, a clear gap exists between the HCHO in southeast and northwest China. The mean HCHO is high over megacity clusters in the southeastern regions, such as the Northern China Plain, Sichuan Basin, Yangtze River Delta, Pearl River Delta, and the Central Yangtze River Plain. More than 45% of the grids show positive trends in satellite HCHO columns in 2013–2021. HCHO columns increase by 0.01% $year^{-1}$, averaged from all grids in 2013–2021 in eastern China. This finding is consistent with the increases in anthropogenic VOC emissions (Zheng et al., 2018b; Zhang et al., 2019). In 2020–2021, satellite-based

270 HCHO decrease in most of eastern China compared to 2019. The changes in HCHO are driven by several factors (Zhu et al., 2017): NOx reductions can lower the HCHO yield from isoprene oxidation (Souri et al., 2020; Wolfe et al., 2016), and in addition, HCHO columns may show interannual variability driven by interannual variability of meteorology, particularly temperature (Duncan et al., 2009; Abbot et al., 2003). Nevertheless, HCHO has not declined as dramatically as NO_2, particularly until 2019. In the NCP, where VOC-limited chemistry most widely exists, the gap between HCHO and NO_2
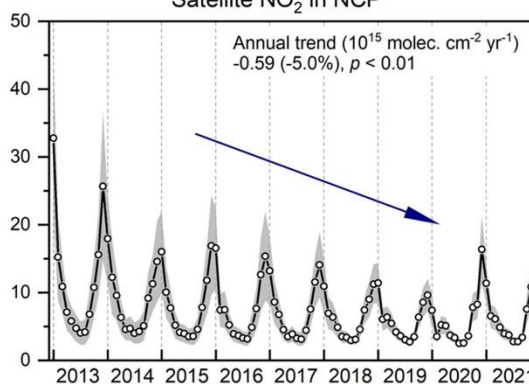
275 changes is even larger.
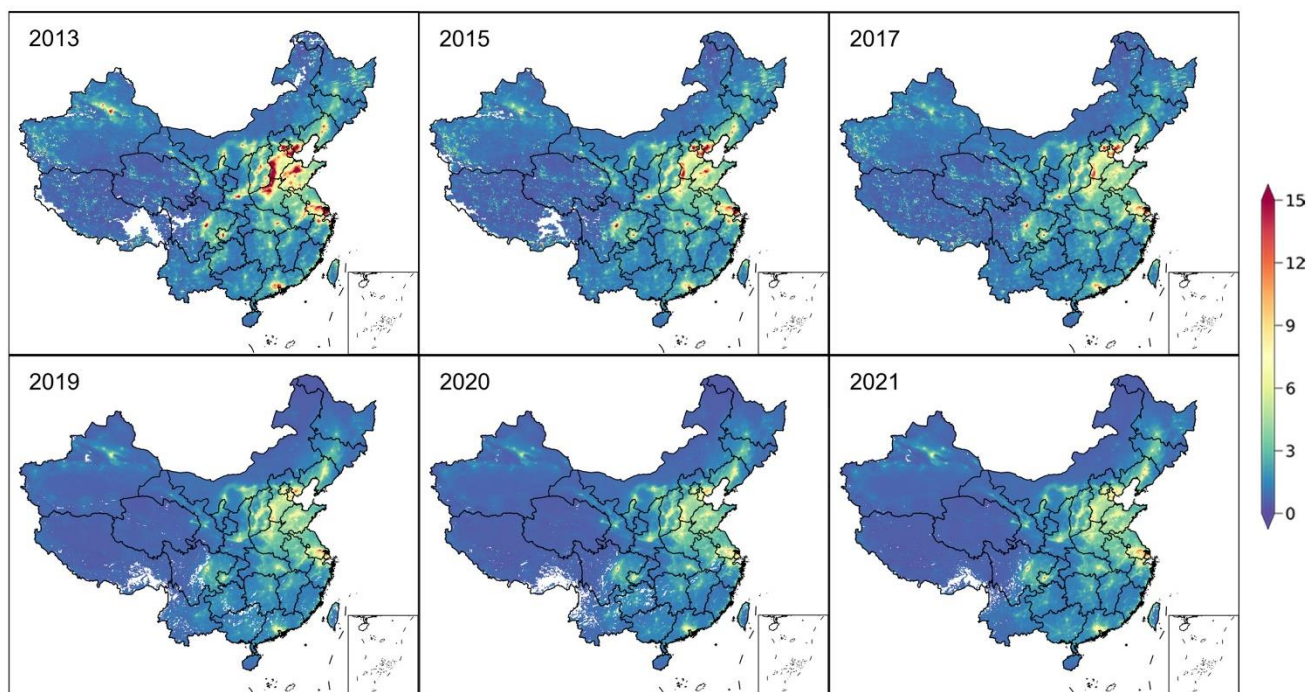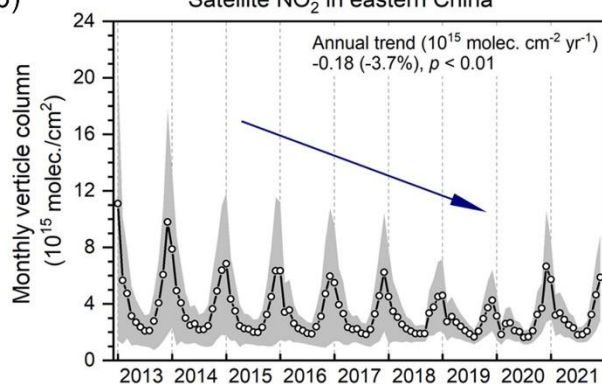
Figure 5: (a) Maps of average satellite-based NO2 columns over China from April to September, and (b) monthly mean NO2 columns averaged over eastern China and North China Plain. Gray shading: mean value ± 50% standard deviation across all grids for each month. Solid line: the linear fitted curve. Inset: absolute annual linear trend and percentage of annual trend (% per year, the linear trend divided by the 2013 mean values).

(a) Satellite HCHO (molec/cm^2)
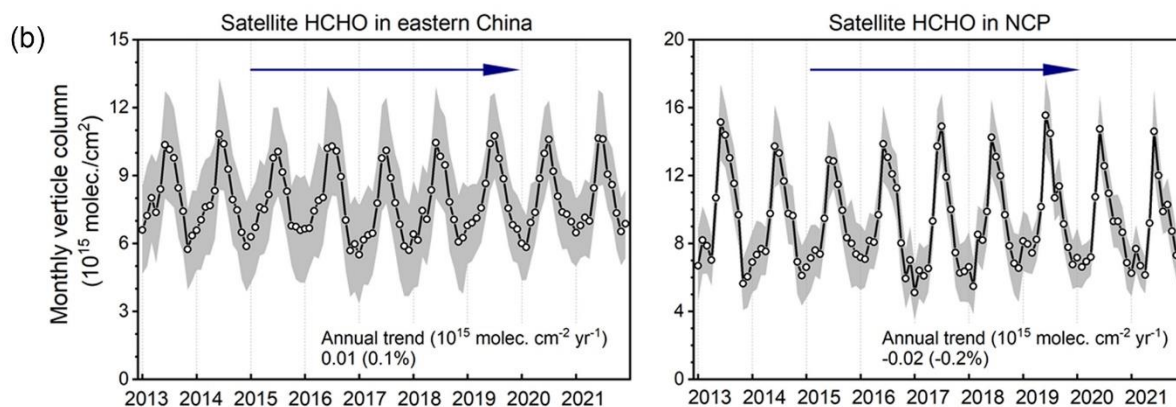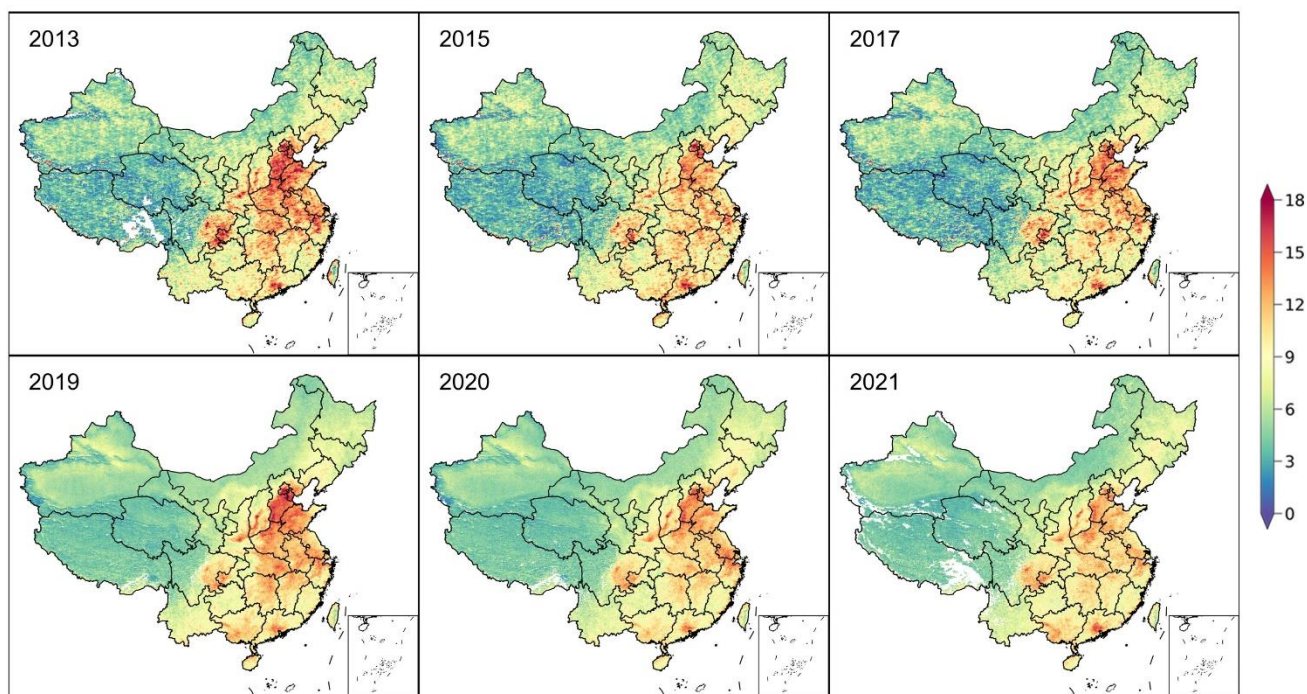
Figure 6: Same as Figure 5 but for satellite-based HCHO columns.

The changes in VOC and NOx emissions presumably have the same disparity as the changes in satellite HCHO and NO$_2$. The anthropogenic NOx emission has been decreased considerably since 2013. However, VOC emissions have not been effectively reduced or even slightly increased. The significant NOx reduction alone without effective VOC control has not worked or has even aggravated O$_3$ pollution in recent years because of the VOC-limited (or NOx-saturated) O$_3$ production regimes in major city clusters.

14

3.4 Cases of O₃ responses to the changes in its precursors

The outbreak of the COVID-19 pandemic produced previously unseen societal impacts in China. Compared to normal
290 years, the measures during the plague prevention and the work resumption resulted in changes in VOC and NO_x emissions in
2020 (Le et al., 2020; Pei et al., 2022). The changes, which are not uniform or synchronized across the country, serve as a
natural experiment to evaluate surface O_3 responses to a marked emission variation.

In Beijing, the capital of China, the average O_3 MDA8 concentration reached 118.9 μg m^{-3} in April 2020, which is 15.5%
and 11.9% higher than that in April 2019 and 2021 (Fig. 7a). The satellite or ground-based observations of NO_2 and HCHO
295 show variations in NOx and VOCs. NO_2 concentrations were the lowest in April 2020 compared with the monthly means in
April 2019 and 2021, showing reductions of 33.2%–42.1% and 17.8%–28.5%. This scenario is associated with a massive
reduction in human activity (Le et al., 2020). Unlike the change in NO_2, HCHO columns in April 2020 are only 16.5% lower
than those in 2019 and even 8.7% higher than those in 2021. In the NOx-saturated (VOC-limited) regime, VOC emission
reductions are generally effective in reducing O_3 concentrations. However, the former is primarily offset by the reduction in
300 NOx emissions resulting in a low titration of O_3 by NOx, which directly increases O_3 combined with the relatively high
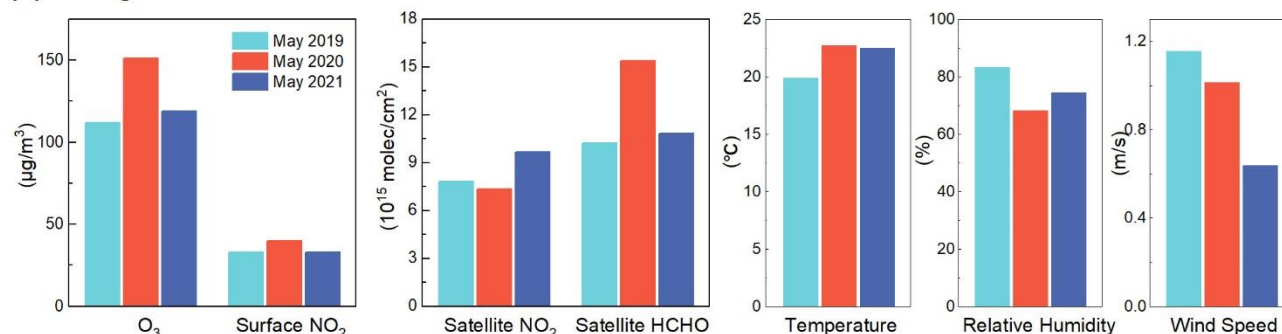temperature and low humidity.
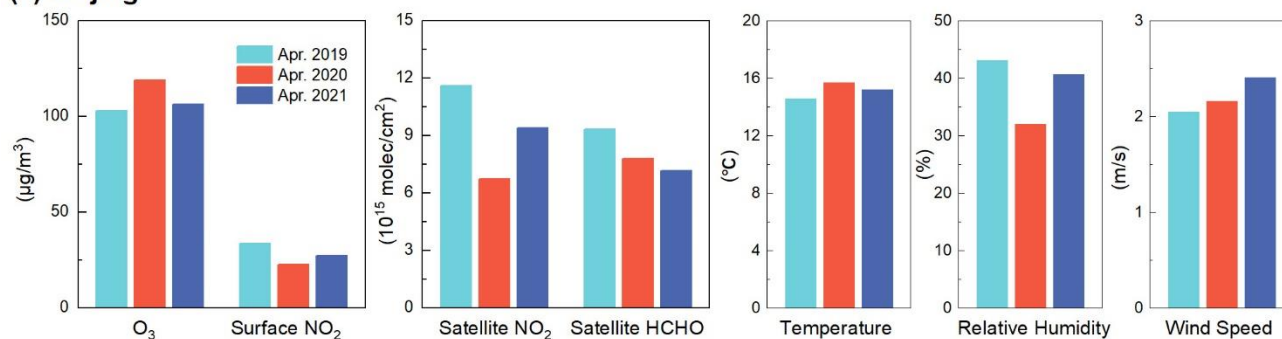
Figure 7: Ground-based observation of O₂ and NO₂, satellite-based NO₂ and HCHO, and meteorological conditions, including temperature, relative humidity and windspeed in (a) Beijing and (b) Chengdu, Sichuan. The figure compares monthly averages 305 for Beijing in April and for Chengdu in May 2019–2021.

Serious ozone pollution occurred in Chengdu, the capital of Sichuan Province, in May 2020, with the maximum hourly ozone concentration reaching 258.8 µg m^{-3}. The monthly average MDA8 is 34.8% and 26.9% higher than that in May 2019 and 2021, respectively. Compared with the monthly means in May 2019 and 2021, the monthly means in May 2020 demonstrate the almost constant NO_2 (−6.1% to 21.2% and −24.3% to 21.2%) and the considerable increase in HCHO (50.7%

310 and 42.2%), as shown in Fig. 7b. As expected, the increase in VOC emissions is a major contributor to the growth of O_3 because of the VOC-limited conditions in Chengdu. This scenario may be related to the vigorous development of stall businesses in Chengdu at that time to help work resumption. These two cases in Beijing and Chengdu verify the negative effect of NOx reduction alone or VOC increase on O_3 pollution in urban cities.

4 Implication

315 Identifying the causes of ozone increases since 2013 is crucial for effectively controlling the ozone pollution in China. The Chinese government has been controlling mainly particulate matter, SO_2, and NOx since 1998 (Zhang et al., 2016). The Air Pollution Prevention and Action Plan, implemented in 2013, aims to reduce the annual average $PM_{2.5}$ concentration by 10% in 2017 compared with 2012 (Chinese State Council, 2013). In 2018, the Chinese government promulgated the Three-Year Action Plan for Winning the Battle of the Blue Sky, which still regards $PM_{2.5}$ control as the primary goal and

320 targets SO_2 and NOx emission reductions (Chinese State Council, 2018). These nationwide emission control measures have decreased $PM_{2.5}$ concentrations rapidly (Xiao et al., 2021) and reduced anthropogenic NOx emissions. However, the decline in VOC emissions is not yet evident. VOC-limited chemistry exists in most city clusters in China, particularly in built-up areas of cities where air quality monitoring sites are located. Our study highlights that the root cause of ozone increase in major regions is the significant reduction of NOx alone without effective control of VOC and not the concurrent decreases in

325 the $PM_{2.5}$ level as suggested in previous studies (Li et al., 2019).

Moreover, the ozone values are high in VOC-limited areas, indicating the necessity of controlling VOC in China. The synergistic control of NOx and VOC, with VOC control as the focus, can help reduce ozone pollution in major cities. The reduction ratio of VOC/NOx can be indicated by the slope of the ridge line of the classic ozone isopleths (Ou et al., 2016; Wang et al., 2019). Based on the method in Fig. 3, O_3 concentrations and the satellite HCHO and NO_2 relationships similar

330 to the O_3 isopleths are obtained. The HCHO/NO_2 value at the peak of the fitted curve is the ratio of HCHO to NO_2 reduction for the fastest decrease in O_3 concentration. Three typical developed cities, namely, Beijing in the NCP, Guangzhou in the PRD, and Chengdu in the SCB, are selected to study the reduction pathways, as shown in Fig. 8. The optimal decrease ratio of HCHO to NO_2 is between 2:1 and 4:1, which is 3.4–3.9 for Beijing, 2.2–2.6 for Chengdu, and 2.3–2.8 for Guangzhou. The results obtained by this method roughly reflect the optimal abatement pathways for the two precursors by using the

335 satellite HCHO and NO_2 to represent VOC and NOx. The short-term future O_3 control becomes much more promising in terms of enhanced VOC control in urban cities dominated by VOC-limited regimes.

Atmospheric
Chemistry
and Physics

Discussions
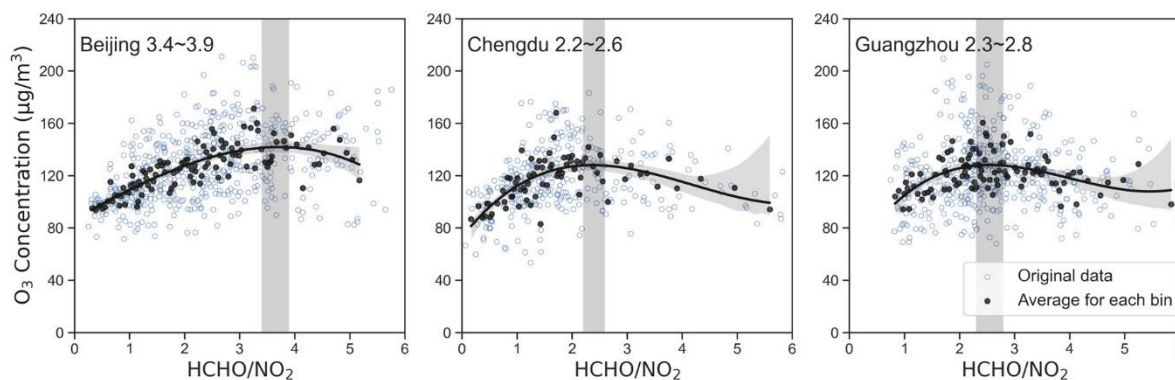
Figure 8: O₃ concentration as a function of HCHO/NO₂ for all sites in Beijing, Chengdu, and Guangzhou. Black dots and lines are the same as those in Figure 3b but divided into 100 bins, and blue circles are original concentrations.

Data availability

The data used in this study can be accessed by contacting the corresponding author, Shaodong Xie (sdxie@pku.edu.cn).

Author contribution

SX and JR initiated the research project and commented on the paper. JR performed the data analyses and wrote the paper.

Competing interests

The authors declare that they have no conflict of interest.

Acknowledgments

This work is supported by the National Key Research and Development Program of China (No. 2018YFC0214001).

References

Abbot, D. S., Palmer, P. I., Martin, R. V., Chance, K. V., Jacob, D. J., and Guenther, A.: Seasonal and interannual variability of North American isoprene emissions as determined by formaldehyde column measurements from space, Geophys. Res. Lett., 30, https://doi.org/10.1029/2003GL017336, 2003.

Atkinson, R.: Atmospheric chemistry of VOCs and NOx, Atmos. Environ., 34, 2063-2101, https://doi.org/10.1016/S1352-2310(99)00460-4, 2000.

355   Action plan on air pollution prevention and control (in Chinese): http://www.gov.cn/zwgk/2013-09/12/content_2486773.htm, (last accessed: 7 March 2022), 2013.

Three-year action plan on defending the blue Sky (in Chinese): http://www.gov.cn/zhengce/content/2018-07/03/content_5303158.htm, (last accessed: 7 March 2022), 2018.

Choi, Y., Kim, H., Tong, D., and Lee, P.: Summertime weekly cycles of observed and modeled NOx and O3 concentrations
360   as a function of satellite-derived ozone production sensitivity and land use types over the Continental United States, Atmos. Chem. Phys., 12, 6291-6307, https://doi.org/10.5194/acp-12-6291-2012, 2012.

Duncan, B. N., Yoshida, Y., Damon, M. R., Douglass, A. R., and Witte, J. C.: Temperature dependence of factors controlling isoprene emissions, Geophys. Res. Lett., 36, https://doi.org/10.1029/2008GL037090, 2009.

Duncan, B. N., Yoshida, Y., Olson, J. R., Sillman, S., Martin, R. V., Lamsal, L., Hu, Y., Pickering, K. E., Retscher, C., Allen,
365   D. J., and Crawford, J. H.: Application of OMI observations to a space-based indicator of NOx and VOC controls on surface ozone formation, Atmos. Environ., 44, 2213-2223, https://doi.org/10.1016/j.atmosenv.2010.03.010, 2010.

Jiang, Z., Jolleys, M. D., Fu, T., Palmer, P. I., Ma, Y., Tian, H., Li, J., and Yang, X.: Spatiotemporal and probability variations of surface PM2.5 over China between 2013 and 2019 and the associated changes in health risks: An integrative observation and model analysis, Sci. Total Environ., 723, 137896, https://doi.org/10.1016/j.scitotenv.2020.137896, 2020.

370   Jin, X., Fiore, A. M., Murray, L. T., Valin, L. C., Lamsal, L. N., Duncan, B., Folkert Boersma, K., De Smedt, I., Abad, G. G., Chance, K., and Tonnesen, G. S.: Evaluating a Space-Based Indicator of Surface Ozone-NOx-VOC Sensitivity Over Midlatitude Source Regions and Application to Decadal Trends, Journal of Geophysical Research: Atmospheres, 122, 10, 410-439, 461, https://doi.org/10.1002/2017JD026720, 2017.

Jin, X., Fiore, A., Boersma, K. F., De Smedt, I., and Valin, L.: Inferring Changes in Summertime Surface Ozone-NOx-VOC
375   Chemistry over US Urban Areas from Two Decades of Satellite and Ground-Based Observations, Environ. Sci. Technol., 54, 6518-6529, https://doi.org/10.1021/acs.est.9b07785, 2020.

Jin, X., and Holloway, T.: Spatial and temporal variability of ozone sensitivity over China observed from the Ozone Monitoring Instrument, Journal of Geophysical Research: Atmospheres, 120, 7229-7246, https://doi.org/10.1002/2015JD023250, 2015.

380   KLEINMAN, L. I.: Low and high NOx tropospheric photochemistry, JOURNAL OF GEOPHYSICAL RESEARCH-ATMOSPHERES, 99, 16831-16838, https://doi.org/10.1029/94JD01028, 1994.

Lamsal, L. N., Krotkov, N. A., Celarier, E. A., Swartz, W. H., Pickering, K. E., Bucsela, E. J., Gleason, J. F., Martin, R. V., Philip, S., Irie, H., Cede, A., Herman, J., Weinheimer, A., Szykman, J. J., and Knepp, T. N.: Evaluation of OMI operational standard NO2 column retrievals using in situ and surface-based NO2 observations, Atmos. Chem. Phys., 14,
385   11587-11609, https://doi.org/10.5194/acp-14-11587-2014, 2014.

Le, T., Wang, Y., Liu, L., Yang, J., Yung, Y. L., Li, G., and Seinfeld, J. H.: Unexpected air pollution with marked emission reductions during the COVID-19 outbreak in China, Science, 369, 702, https://doi.org/10.1126/science.abb7431, 2020.

Li, D. R., Wang, S. S., Xue, R. B., Zhu, J., Zhang, S. B., Sun, Z. B., and Zhou, B.: OMI-observed HCHO in Shanghai, China,

during 2010-2019 and ozone sensitivity inferred by an improved HCHO/NO2 ratio, Atmos. Chem. Phys., 21, 15447-

390   15460, https://doi.org/10.5194/acp-21-15447-2021, 2021.

Li, K., Jacob, D. J., Liao, H., Shen, L., Zhang, Q., and Bates, K. H.: Anthropogenic drivers of 2013-2017 trends in summer surface ozone in China, P. Natl. Acad. Sci. Usa., 116, 422-427, https://doi.org/10.1073/pnas.1812168116, 2019.

Lin, N., Wang, Y., Zhang, Y., and Yang, K.: A large decline of tropospheric NO2 in China observed from space by SNPP OMPS, Sci. Total Environ., 675, 337-342, https://doi.org/10.1016/j.scitotenv.2019.04.090, 2019.

395   Liu, C., and Shi, K.: A review on methodology in O3-NOx-VOC sensitivity study, Environ. Pollut., 291, https://doi.org/10.1016/j.envpol.2021.118249, 2021.

Lu, X., Hong, J., Zhang, L., Cooper, O. R., Schultz, M. G., Xu, X., Wang, T., Gao, M., Zhao, Y., and Zhang, Y.: Severe Surface Ozone Pollution in China: A Global Perspective, Environmental Science & Technology Letters, 5, 487-494, https://doi.org/10.1021/acs.estlett.8b00366, 2018.

400   Lu, X., Zhang, L., Wang, X., Gao, M., Li, K., Zhang, Y., Yue, X., and Zhang, Y.: Rapid Increases in Warm-Season Surface Ozone and Resulting Health Impact in China Since 2013, Environmental Science & Technology Letters, 7, 240-247, https://doi.org/10.1021/acs.estlett.0c00171, 2020.

Martin, R. V.: Global inventory of nitrogen oxide emissions constrained by space-based observations of NO2 columns, Journal of Geophysical Research, 108, https://doi.org/10.1029/2003JD003453, 2003.

405   Martin, R. V., Fiore, A. M., and Van Donkelaar, A.: Space-based diagnosis of surface ozone sensitivity to anthropogenic emissions, Geophys. Res. Lett., 31, https://doi.org/10.1029/2004GL019416, 2004.

Nelson, B. S., Stewart, G. J., Drysdale, W. S., Newland, M. J., Vaughan, A. R., Dunmore, R. E., Edwards, P. M., Lewis, A. C., Hamilton, J. F., Acton, W. J., Hewitt, C. N., Crilley, L. R., Alam, M. S., Sahin, U. A., Beddows, D. C. S., Bloss, W. J., Slater, E., Whalley, L. K., Heard, D. E., Cash, J. M., Langford, B., Nemitz, E., Sommariva, R., Cox, S., Shivani, Gadi, R.,

410   Gurjar, B. R., Hopkins, J. R., Rickard, A. R., and Lee, J. D.: In situ ozone production is highly sensitive to volatile organic compounds in Delhi, India, Atmos. Chem. Phys., 21, 13609-13630, https://doi.org/10.5194/acp-21-13609-2021, 2021.

Ou, J., Yuan, Z., Zheng, J., Huang, Z., Shao, M., Li, Z., Huang, X., Guo, H., and Louie, P. K. K.: Ambient Ozone Control in a Photochemically Active Region: Short-Term Despiking or Long-Term Attainment? Environ. Sci. Technol., 50, 5720-

415   5728, https://doi.org/10.1021/acs.est.6b00345, 2016.

Pei, C., Yang, W., Zhang, Y., Song, W., Xiao, S., Wang, J., Zhang, J., Zhang, T., Chen, D., Wang, Y., Chen, Y., and Wang, X.: Decrease in ambient volatile organic compounds during the COVID-19 lockdown period in the Pearl River Delta region, south China., The Science of the total environment, 153720, https://doi.org/10.1016/j.scitotenv.2022.153720, 2022.

420   Pusede, S. E., Steiner, A. L., and Cohen, R. C.: Temperature and Recent Trends in the Chemistry of Continental Surface Ozone, Chem. Rev., 115, 3898-3918, https://doi.org/10.1021/cr5006815, 2015.

Pusede, S. E., and Cohen, R. C.: On the observed response of ozone to NOx and VOC reactivity reductions in San Joaquin

Atmospheric
Chemistry
and Physics
Discussions

Valley California 1995-present, Atmos. Chem. Phys., 12, 8323-8339, https://doi.org/10.5194/acp-12-8323-2012, 2012.

Ren, J., Hao, Y., Simayi, M., Shi, Y., and Xie, S.: Spatiotemporal variation of surface ozone and its causes in Beijing, China
425   since 2014, Atmos. Environ., 260, https://doi.org/10.1016/j.atmosenv.2021.118556, 2021.

Schroeder, J. R., Crawford, J. H., Fried, A., Walega, J., Weinheimer, A., Wisthaler, A., Muller, M., Mikoviny, T., Chen, G.,
Shook, M., Blake, D. R., and Tonnesen, G. S.: New insights into the column CH2O/NO2 ratio as an indicator of near-
surface ozone sensitivity, JOURNAL OF GEOPHYSICAL RESEARCH-ATMOSPHERES, 122, 8885-8907,
https://doi.org/10.1002/2017JD026781, 2017.

430   Shen, H., Sun, Z., Chen, Y., Russell, A. G., Hu, Y., Odman, M. T., Qian, Y., Archibald, A. T., and Tao, S.: Novel Method
for Ozone Isopleth Construction and Diagnosis for the Ozone Control Strategy of Chinese Cities, Environ. Sci. Technol.,
55, 15625-15636, https://doi.org/10.1021/acs.est.1c01567, 2021.

Shen, L., Jacob, D. J., Zhu, L., Zhang, Q., Zheng, B., Sulprizio, M. P., Li, K., De Smedt, I., Abad, G. G., Cao, H., Fu, T., and
Liao, H.: The 2005-2016 Trends of Formaldehyde Columns Over China Observed by Satellites: Increasing
435   Anthropogenic Emissions of Volatile Organic Compounds and Decreasing Agricultural Fire Emissions, Geophys. Res.
Lett., 46, 4468-4475, https://doi.org/10.1029/2019GL082172, 2019.

SILLMAN, S.: THE USE OF NOY, H2O2, AND HNO3 AS INDICATORS FOR OZONE-NOX-HYDROCARBON
SENSITIVITY IN URBAN LOCATIONS, JOURNAL OF GEOPHYSICAL RESEARCH-ATMOSPHERES, 100,
14175-14188, https://doi.org/10.1029/94JD02953, 1995.

440   Sillman, S.: The relation between ozone, NOx and hydrocarbons in urban and polluted rural environments, Atmos. Environ.,
33, 1821-1845, https://doi.org/10.1016/S1352-2310(98)00345-8, 1999.

Sillman, S., Logan, J. A., and Wofsy, S. C.: The sensitivity of ozone to nitrogen oxides and hydrocarbons in regional ozone
episodes, Journal of Geophysical Research: Atmospheres, 95, 1837-1851, https://doi.org/10.1029/JD095iD02p01837,
1990.

445   Sillman, S., and He, D. Y.: Some theoretical results concerning O-3-NOx-VOC chemistry and NOx-VOC indicators,
JOURNAL OF GEOPHYSICAL RESEARCH-ATMOSPHERES, 107, https://doi.org/10.1029/2001JD001123, 2002.

Simayi, M., Shi, Y., Xi, Z., Ren, J., Hini, G., and Xie, S.: Emission trends of industrial VOCs in China since the clean air
action   and   future   reduction   perspectives,   Sci.   Total   Environ.,   826,   153994,
https://doi.org/10.1016/j.scitotenv.2022.153994, 2022.

450   Souri, A. H., Nowlan, C. R., Wolfe, G. M., Lamsal, L. N., Chan Miller, C. E., Abad, G. G., Janz, S. J., Fried, A., Blake, D.
R., Weinheimer, A. J., Diskin, G. S., Liu, X., and Chance, K.: Revisiting the effectiveness of HCHO/NO2 ratios for
inferring ozone sensitivity to its precursors using high resolution airborne remote sensing observations in a high ozone
episode   during   the   KORUS-AQ   campaign,   Atmos.   Environ.,   224,   117341,
https://doi.org/10.1016/j.atmosenv.2020.117341, 2020.

455   Tan, Z., Hofzumahaus, A., Lu, K., Brown, S. S., Holland, F., Huey, L. G., Kiendler-Scharr, A., Li, X., Liu, X., Ma, N., Min,
K., Rohrer, F., Shao, M., Wahner, A., Wang, Y., Wiedensohler, A., Wu, Y., Wu, Z., Zeng, L., Zhang, Y., and Fuchs, H.:

No Evidence for a Significant Impact of Heterogeneous Chemistry on Radical Concentrations in the North China Plain in Summer 2014, Environ. Sci. Technol., 54, 5973-5979, https://doi.org/10.1021/acs.est.0c00525, 2020.

Tan, Z., Lu, K., Jiang, M., Su, R., Dong, H., Zeng, L., Xie, S., Tan, Q., and Zhang, Y.: Exploring ozone pollution in Chengdu, southwestern China: A case study from radical chemistry to O3-VOC-NOx sensitivity, Sci. Total Environ., 636, 775-786, https://doi.org/10.1016/j.scitotenv.2018.04.286, 2018.

Wang, N., Lyu, X., Deng, X., Huang, X., Jiang, F., and Ding, A.: Aggravating O3 pollution due to NOx emission control in eastern China, Sci. Total Environ., 677, 732-744, https://doi.org/10.1016/j.scitotenv.2019.04.388, 2019.

Wang, T., Xue, L., Brimblecombe, P., Lam, Y. F., Li, L., and Zhang, L.: Ozone pollution in China: A review of concentrations, meteorological influences, chemical precursors, and effects, Sci. Total Environ., 575, 1582-1596, https://doi.org/10.1016/j.scitotenv.2016.10.081, 2017.

Wang, X., Fu, T., Zhang, L., Cao, H., Zhang, Q., Ma, H., Shen, L., Evans, M. J., Ivatt, P. D., Lu, X., Chen, Y., Zhang, L., Feng, X., Yang, X., Zhu, L., and Henze, D. K.: Sensitivities of Ozone Air Pollution in the Beijing－Tianjin－Hebei Area to Local and Upwind Precursor Emissions Using Adjoint Modeling, Environ. Sci. Technol., 55, 5752-5762, https://doi.org/10.1021/acs.est.1c00131, 2021.

Williams, J. E., Boersma, K. F., Le Sager, P., and Verstraeten, W. W.: The high-resolution version of TM5-MP for optimized satellite retrievals: description and validation, Geosci. Model Dev., 10, 721-750, https://doi.org/10.5194/gmd-10-721-2017, 2017.

Wolfe, G. M., Kaiser, J., Hanisco, T. F., Keutsch, F. N., de Gouw, J. A., Gilman, J. B., Graus, M., Hatch, C. D., Holloway, J., Horowitz, L. W., Lee, B. H., Lerner, B. M., Lopez-Hilifiker, F., Mao, J., Marvin, M. R., Peischl, J., Pollack, I. B., Roberts, J. M., Ryerson, T. B., Thornton, J. A., Veres, P. R., and Warneke, C.: Formaldehyde production from isoprene oxidation across NOx regimes, Atmos. Chem. Phys., 16, 2597-2610, https://doi.org/10.5194/acp-16-2597-2016, 2016.

World Health Organization: WHO's global air-quality guidelines0140-6736, 2021.

Xiao, Q., Geng, G., Xue, T., Liu, S., Cai, C., He, K., and Zhang, Q.: Tracking PM2.5 and O-3 Pollution and the Related Health Burden in China 2013-2020, Environ. Sci. Technol., https://doi.org/10.1021/acs.est.1c04548, 2021.

Yang, L., Luo, H., Yuan, Z., Zheng, J., Huang, Z., Li, C., Lin, X., Louie, P. K. K., Chen, D., and Bian, Y.: Quantitative impacts of meteorology and precursor emission changes on the long-term trend of ambient ozone over the Pearl River Delta, China, and implications for ozone control strategy, Atmos. Chem. Phys., 19, 12901-12916, https://doi.org/10.5194/acp-19-12901-2019, 2019.

Zhang, H., Wang, S., Hao, J., Wang, X., Wang, S., Chai, F., and Li, M.: Air pollution and control action in Beijing, J. Clean. Prod., 112, 1519-1527, https://doi.org/10.1016/j.jclepro.2015.04.092, 2016.

Zhang, Q., Zheng, Y., Tong, D., Shao, M., Wang, S., Zhang, Y., Xu, X., Wang, J., He, H., Liu, W., Ding, Y., Lei, Y., Li, J., Wang, Z., Zhang, X., Wang, Y., Cheng, J., Liu, Y., Shi, Q., Yan, L., Geng, G., Hong, C., Li, M., Liu, F., Zheng, B., Cao, J., Ding, A., Gao, J., Fu, Q., Huo, J., Liu, B., Liu, Z., Yang, F., He, K., and Hao, J.: Drivers of improved PM2.5 air quality in China from 2013 to 2017, P. Natl. Acad. Sci. Usa., 116, 24463-24469, https://doi.org/10.1073/pnas.1907956116, 2019.

Zhao, S., Yin, D., Yu, Y., Kang, S., Qin, D., and Dong, L.: PM2.5 and O3 pollution during 2015 – 2019 over 367 Chinese cities: Spatiotemporal variations, meteorological and topographical impacts, Environ. Pollut., 264, 114694, https://doi.org/10.1016/j.envpol.2020.114694, 2020.

Zheng, B., Tong, D., Li, M., Liu, F., Hong, C., Geng, G., Li, H., Li, X., Peng, L., Qi, J., Yan, L., Zhang, Y., Zhao, H., Zheng, Y., He, K., and Zhang, Q.: Trends in China's anthropogenic emissions since 2010 as the consequence of clean air actions, Atmos. Chem. Phys., 18, 14095-14111, https://doi.org/10.5194/acp-18-14095-2018, 2018a.

Zheng, B., Tong, D., Li, M., Liu, F., Hong, C., Geng, G., Li, H., Li, X., Peng, L., Qi, J., Yan, L., Zhang, Y., Zhao, H., Zheng, Y., He, K., and Zhang, Q.: Trends in China's anthropogenic emissions since 2010 as the consequence of clean air actions, Atmos. Chem. Phys., 18, 14095-14111, https://doi.org/10.5194/acp-18-14095-2018, 2018b.

Zhu, L., Jacob, D. J., Mickley, L. J., Marais, E. A., Cohan, D. S., Yoshida, Y., Duncan, B. N., Abad, G. G., and Chance, K. V.: Anthropogenic emissions of highly reactive volatile organic compounds in eastern Texas inferred from oversampling of satellite (OMI) measurements of HCHO columns, Environ. Res. Lett., 9, https://doi.org/10.1088/1748-9326/9/11/114004, 2014.

Zhu, L., Mickley, L. J., Jacob, D. J., Marais, E. A., Sheng, J., Hu, L., Abad, G. G., and Chance, K.: Long-term (2005-2014) trends in formaldehyde (HCHO) columns across North America as seen by the OMI satellite instrument: Evidence of changing emissions of volatile organic compounds, Geophys. Res. Lett., 44, 7079-7086, https://doi.org/10.1002/2017GL073859, 2017.